

Slice-Level Scheduling for High Throughput and Load Balanced LLM Serving

Ke Cheng*

Nanjing University

Nanjing, China

ketonmi@outlook.com

Hongen Peng

Ant Group

Hangzhou, China

hongan.phe@antgroup.com

Wen Hu

Ant Group

Hangzhou, China

huwen.hu@antgroup.com

Jianguo Li†

Ant Group

Hangzhou, China

lijg.zero@antgroup.com

Zhi Wang

Ant Group

Hangzhou, China

wangchun.wz@antgroup.com

Sheng Zhang†

Nanjing University

Nanjing, China

sheng@nju.edu.cn

ABSTRACT

Large language models (LLMs) iteratively generate text token by token, with memory usage increasing with the length of generated token sequences. The unpredictability of generation lengths makes it difficult to estimate the time and memory needed to process requests, posing a challenge for effective request scheduling. Conventional sequence-level scheduling (SLS) serves requests in a first-come first-served (FCFS) manner with static batching where requests with short generation lengths are delayed until those with long ones have finished generation, which hurts computational efficiency. Besides, to avoid out-of-memory (OOM) errors, SLS batches requests with a small batch size, which limits throughput. Recently proposed iteration-level scheduling (ILS) enhances computational efficiency with continuous batching to return completed requests timely and dynamically add new requests for processing. However, many ILS schedulers limit the number of parallel-processing requests to avoid OOM errors while achieving a fast inference speed, which compromises throughput. Moreover, existing SLS and ILS schedulers fail to balance the workload across multiple deployed LLM instances. To tackle these challenges, we propose slice-level scheduling (SCLS). By splitting the predefined maximal generation length limit into slices and serving batches slice by slice, it provides a precise range of serving time and memory usage for batched requests, laying the foundation for effective scheduling. Experiments confirm that compared with SLS and ILS schedulers, SCLS can improve throughput by up to 315.8% and greatly mitigate load imbalance with proposed batching and offloading algorithms.

PVLDB Reference Format:

Ke Cheng, Wen Hu, Zhi Wang, Hongen Peng, Jianguo Li, and Sheng Zhang. Slice-Level Scheduling for High Throughput and Load Balanced LLM Serving. PVLDB, 14(1): XXX-XXX, 2024.

doi:XX.XX/XXX.XX

*Work done during an internship at Ant Group.

†Jianguo Li and Sheng Zhang are corresponding authors.

This work is licensed under the Creative Commons BY-NC-ND 4.0 International License. Visit <https://creativecommons.org/licenses/by-nc-nd/4.0/> to view a copy of this license. For any use beyond those covered by this license, obtain permission by emailing info@vldb.org. Copyright is held by the owner/author(s). Publication rights licensed to the VLDB Endowment.

Proceedings of the VLDB Endowment, Vol. 14, No. 1 ISSN 2150-8097.
doi:XX.XX/XXX.XX

1 INTRODUCTION

With increasing the parameter size, generative large language models (LLMs) have demonstrated remarkable capabilities across a wide range of SQL-related tasks, such as natural language to SQL, SQL interpretation, and SQL optimization. These advancements greatly benefit LLM-based conversational code-assistant agents like CodeFuse [1] developed by Ant Group. Besides SQL, CodeFuse is also widely acclaimed for its ability to generate, optimize, and interpret various programming languages including Java, Python, and C++, boasting a peak concurrent usage with thousands of online users. Therefore, an efficient serving system with high throughput and scalability is essential to handle such a heavy workload.

LLMs generate tokens iteratively, one per iteration until the terminator end-of-sequence (EOS) token is generated. The number of iterations required to generate the EOS token is referred to as the request generation length. To prevent the generation process from being too long, a maximal generation length limit is always set. When this limit is reached, even if the EOS token has not been generated, the generated results will be returned to users. Moreover, due to the key-value cache that is always leveraged to accelerate LLM inference, the GPU memory consumption increases with the increased number of generated tokens. Therefore, the generation length of a request determines the computational overhead and the memory it consumes in the generation process.

To achieve high throughput for LLM serving, it is significant to fully utilize the parallel computing capability of GPUs with batch serving. Static batching and continuous batching are two batch-serving techniques for LLMs. Static batching pads the raw input of batched requests to the same length before serving and iteratively generates tokens until all requests generate the EOS token or the predefined iteration number limit is reached. Continuous batching leverages customized CUDA kernels to remove request padding and enable dynamic exits and joins of requests during batch serving. However, since the request generation length is unpredictable, it is difficult to estimate the computational overhead and memory consumption of requests. Hence, it is challenging to schedule requests to take full advantage of these batch-serving techniques.

Existing deep learning serving systems [2, 3] adopt the sequence-level scheduling (SLS) to batch requests in a first-come first-served (FCFS) manner with a fixed batch size and serve them with static batching as shown in Fig. 1a, which leads to severe computational

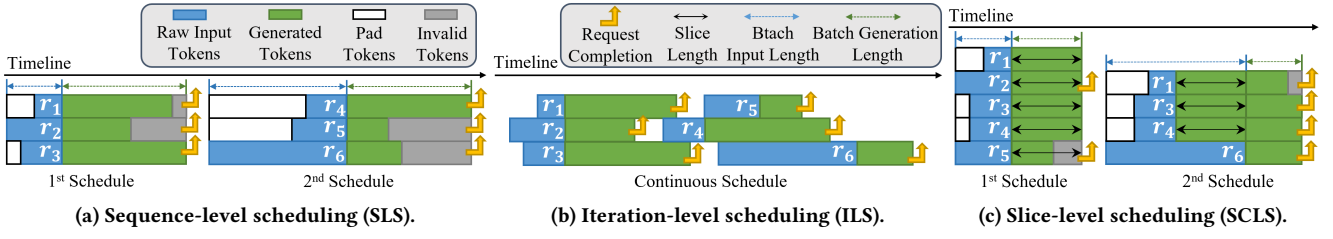


Figure 1: Illustration of various scheduling techniques, where r_i represents the i th arrived request.

inefficiencies. Firstly, without knowing request generation lengths, the SLS scheduler directly sets the iteration number limit for static batching to the predefined maximal generation length and defaults to a small batch size to prevent out-of-memory (OOM) errors, thus failing to fully exploit the GPU’s parallel computing capability and compromising throughput. Secondly, in a batch, requests with short inputs are padded and requests with short outputs have to wait for those with long outputs to finish before they are returned together. Besides, during the waiting, completed requests still participate in the computation and generate invalid tokens.

To eliminate the request padding and waiting caused by SLS and improve computational efficiency, iteration-level scheduling (ILS) is introduced in recent studies [4–6]. Current ILS techniques leverage continuous batching to timely return completed requests and add newly arrived requests for processing in an FCFS manner at each iteration as shown in Fig. 1b. However, without knowing request generation lengths, many ILS techniques [4, 6] adopt conservative memory management strategies that limit the number of parallel-processing requests to avoid OOM errors and speed up inference, thus under-utilizing the GPU and hurting throughput.

Moreover, existing SLS and ILS schedulers [2, 3, 6] leverage the round-robin policy to offload requests to multiple LLM instances, which can cause unbalanced distribution of computational overhead and memory consumption across LLM instances due to the variance of request generation lengths.

In this paper, we propose slice-level scheduling (SCLS) to address the aforementioned challenges from a pure scheduling perspective. The core idea is to split the predefined maximal generation length limit into fixed-length slices and serve batches slice by slice. Requests that complete their generation are returned, while incomplete requests are rescheduled with newly arrived requests until finished. SCLS can integrate with both static and continuous batching. We focus on the integration with static batching in this paper and discuss the integration with continuous batching in Section 7.

By setting the iteration number limit of static batching to the slice length, requests with short generation lengths can be returned in a few slices without waiting for long. Besides, compared with the predefined maximal generation length, the small slice length results in a narrow range of generation length at each schedule, thus providing a precise range of memory consumption and serving time for batches. Therefore, with the precise range of memory consumption, requests can be adaptively batched together with as large a batch size as possible to improve the throughput without exceeding GPU memory as shown in Fig. 1c. Moreover, with the precise range of serving time, batches can be scheduled to LLM instances using the max-min policy [7] to achieve load-balancing. All in all, generation slicing lays the foundation for effective scheduling.

We implement a prototype system of SCLS and conduct extensive experiments with 8 LLaMA2-13B instances deployed on 8 NVIDIA A100 80GB GPUs. The experimental results show that SCLS can achieve a high request throughput and a more balanced workload across LLM instances. Our main contribution is listed as follows.

- We demonstrate the inefficiency and load imbalance of existing SLS and ILS schedulers through experiments. Besides, we find that requests with long outputs are rare by analyzing the ShareGPT dataset and request traces collected from CodeFuse logs. These motivate the birth of SCLS.
- We propose SCLS. By limiting the number of iterations to a small slice length in each schedule, it controls the serving time and memory usage of batches to a precise range, laying the foundation for effective scheduling.
- We design a dynamic programming-based batching algorithm and a max-min-based offloading algorithm for SCLS. They divide requests into batches to minimize the batch serving time and balance the computational workload across multiple LLM instances, respectively.
- We conduct extensive experiments to confirm the superiority of SCLS. Equipped with various inference engines, SCLS can improve request throughput by up to 315.8% and reduce response time by up to 91.1% compared with existing SLS and ILS schedulers under the CodeFuse request trace.

2 PRELIMINARIES

2.1 Autoregressive Language Model Generation

Language models take a token sequence as input to predict the probability distribution over the vocabulary for the next token. By sampling from the distribution, a new token is generated. Hence, a sequence of tokens can be generated by iteratively adding the newly generated token at the end of the input sequence and re-feeding the sequence to the language model. Such a generation pattern is called autoregressive generation.

The autoregressive generation stops when the EOS token is generated or the predefined maximal generation length limit is reached. In this paper, the process of generating one token is termed an iteration. The length (i.e., number of tokens) of the raw request text is termed as the **request input length**. Besides, we term the number of iterations until the EOS token is output as the **request generation length**.

2.2 Large Language Model Inference Procedure

Current popular LLMs such as GPT, LLaMA, LLaMA2, Qwen, and ChatGLM [8–13] all adopt the decoder-only transformer architecture whose computation flow is depicted in Fig. 2.

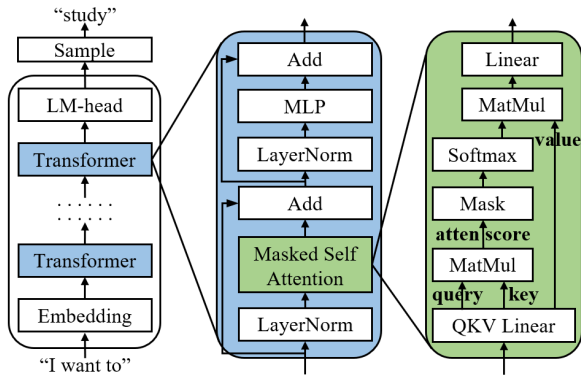


Figure 2: LLM inference procedure. The blue and green rounded rectangles depict the computation flow of the transformer block and masked-self attention, respectively.

After feeding the text "I want to" to the LLM, the input token sequence is successively processed by a linear layer called embedding, a stack of transformer blocks, a linear layer called lm-head, and finally a possibility distribution is produced, from which "study" is sampled as the next token.

The most significant part of LLMs is the transformer block, of which the masked self-attention module is the core component that elevates it [14]. As shown in Fig. 2, for each token in the input sequence, the self-attention module first derives three tensors, which are query, key, and value. After that, the query matrix and key matrix are multiplied to yield the attention-score matrix, which represents the correlation between tokens. Since LLMs are trained to predict the next token, each input token should not see information after its location. Therefore, a mask operation is performed on the attention-score matrix, where a very large negative number is added to the attention scores that represent the correlation between tokens and their successive tokens. Therefore, these attention scores become negligible in the relevant matrix obtained after the soft-max operation. Next, by multiplying the relevant matrix with the value matrix, each token can extract features from its preceding tokens to update itself.

2.3 Key-Value Cache and Two-Phase Inference

In a stateless implementation of LLM autoregressive generation, each transformer block computes key and value tensors for all input tokens in each iteration, resulting in significant computational overhead. This overhead escalates in autoregressive generation because newly generated tokens are continuously appended to the input sequence, which incrementally increases the per-iteration computational overhead.

To alleviate such a severe overhead, existing inference engines such as huggingface-transformers [15] and deepspeed-inference [16] cache the computed key and value tensors in GPU memory. As shown in Fig. 3, in the first iteration, the origin input sequence is fed to the LLM and the corresponding key and value tensors are computed and cached. In subsequent iterations, only the latest generated token is fed to the LLM for computation and cache of key and value tensors, which significantly cuts down the computational overhead. Accordingly, the inference process can be split into two phases. The first iteration is the **prefill phase**, which involves

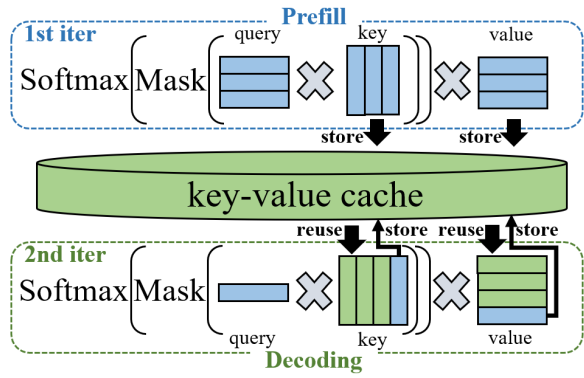


Figure 3: Key-value cache usage in two phases. The raw request has 3 tokens and the blue and green grids represent the newly derived and reused key and value tensors, respectively.

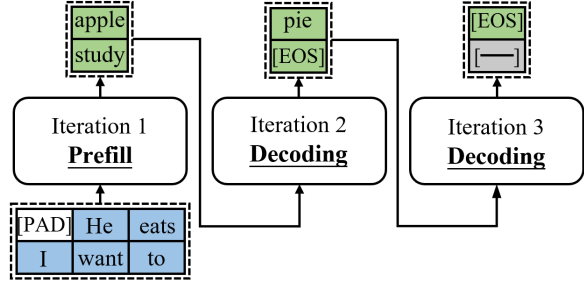


Figure 4: Static batching example. The blue and green grids represent raw input tokens of the requests and valid tokens generated by the LLM, respectively.

intensive key and value computation for all raw input tokens of the request, hence computationally heavy. Subsequent iterations are the **decoding phase**, which only computes key and value tensors for the input token, hence computationally light.

2.4 Serving Requests with Static Batching

Fig. 4 illustrates the serving process of static batching. Firstly, all the batched requests are padded to the same length as the longest one using the pad token. Next, the batch is fed to the LLM to generate tokens autoregressively. To prevent the pad token from being attended by other tokens, the corresponding attention score is also masked during the inference process. Until all the requests generate the EOS token or the preset iteration number limit is reached, the serving process completes. Since the generation lengths of requests in a batch are diverse, the requests that generate the EOS token early continue generating invalid tokens until the serving process completes, but the tokens generated after the EOS token will be ignored in the response.

In this paper, we refer to the longest raw input length of requests in a batch as the **batch input length**, which is equal to the token sequence length of each request after padding. Moreover, we take the minimum of the preset iteration number limit and the longest generation length of requests in a batch as the **batch generation length**, which is equal to the total number of iterations in the batch serving procedure.

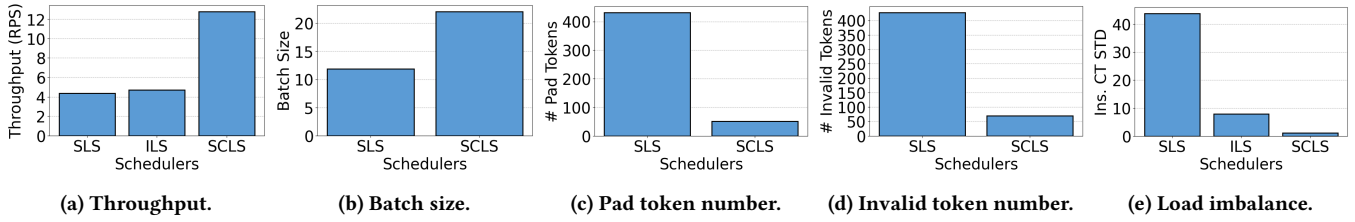


Figure 5: Inefficiency and load imbalance of SLS and ILS schedulers. Sub-figures (a) and (e) show that SCLS can significantly outperform SLS and ILS schedulers in terms of throughput and load balancing. Sub-figures (b)~(d) present that SCLS’s superior performance comes from the increase of batch size and decrease of the number of pad tokens and invalid tokens.

3 MOTIVATION

3.1 Inefficient Serving of SLS and ILS

We conduct an experiment to confirm the inefficient serving of SLS and ILS schedulers. We implement the SLS and SCLS schedulers using the deepspeed-inference-v0.13.3 as the inference engine and leverage the deepspeed-fastgen-v0.2.0 as the ILS scheduler. In the experiment, 8 LLaMA2-13B instances are deployed on 8 NVIDIA A100 80GB GPUs, and requests with various input and generation lengths arrive at a rate of 20 per second. Other settings are the same as in Section 5. The experimental results are shown in Fig. 5.

From Fig. 5a, we can see that the throughput of SLS is much smaller than that of SCLS. This is because SLS serves requests with a fixed small batch size, which wastes the powerful parallel computing capability of GPUs. Moreover, SLS batches requests in an FCFS manner, which leads to a lot of pad tokens and incurs additional computational overhead. Furthermore, setting the iteration number limit of static batching directly to the maximal generation length limit causes many requests can not be returned in time and a large number of invalid tokens are generated.

Although the continuous batching can eliminate pad tokens and invalid tokens in the serving process, the throughput of ILS is also much lower than that of SCLS, because the ILS scheduler adopts a conservative memory management mechanism that limits the number of parallel-processing requests. Therefore, the ILS scheduler can not fully utilize the parallel computing capability of GPUs, resulting in a low throughput.

3.2 Unbalanced Workload of SLS and ILS

We record the time when each LLM instance completes serving at the end of the experiment and depict the standard deviation (STD) of the completion time (CT) of instances in Fig. 5e.

Since both SLS and ILS schedulers use the round-robin policy to offload requests, requests with long generation lengths and requests with short generation lengths may be assigned to different instances, resulting in unbalanced memory consumption and computational overhead across instances. For the SLS scheduler, instances that have more requests with long generation lengths take more time to serve requests. For the ILS scheduler, instances that have more requests with long generation lengths consume more memory and cannot often add new requests for processing due to insufficient memory, causing a long request queuing time. Such a load imbalance accumulates to result in a large variance in the completion time of LLM instances. Hence, the standard deviation of instance completion time of SLS and ILS is much larger than that of SCLS.

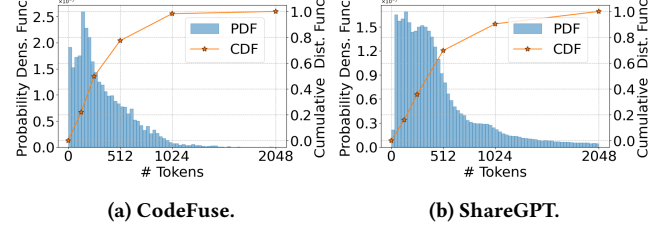


Figure 6: Probability density function (PDF) and cumulative distribution function (CDF) of the request generation length in actual scenarios.

3.3 Actual Generation Length Distribution

To understand the generation length distribution in actual scenarios, we analyze the request data of CodeFuse and ShareGPT. CodeFuse [1] is a chatbot developed by Ant Group that is optimized for generating, interpreting, and optimizing program code. We collected user request trace from CodeFuse’s logs for October and November 2023, and depict the distribution of request generation lengths in Fig. 6a. ShareGPT [17] is a publicly available website that shares conversations from users chatting with ChatGPT [18]. We analyze close to 400,000 pieces of data collected from ShareGPT and present the generation length distribution in Fig. 6b.

From Fig. 6, we can find that the vast majority of requests have a small generation length of less than 512 in both the CodeFuse and ShareGPT data. Hence, for static batching, if we split the maximal generation length limit (e.g., 2048) into slices with a small slice length (e.g., 128) and serve batched requests slice by slice, most requests can be returned in time within a small number of slices. In addition, since the iteration number limit is set to the small slice length, we can get a precise range of memory consumption and batch together as many uncompleted requests and newly arrived requests as possible while ensuring that OOM errors will not occur, thus increasing throughput and achieving efficient batch serving.

Moreover, we can also get a precise range of batch serving time as well. Therefore, load balancing can be achieved by offloading batches with the max-min policy where the batch with the longest serving time is offloaded to the least loaded instance.

Considering the above, we propose SCLS, which splits the pre-defined maximal generation length limit into fixed-length slices, limits the number of iterations in each batch serving to the slice length and serves requests slice by slice. Although requests with long generation lengths suffer from the extra overhead of recomputing the prefill phase at every reschedule, the overhead is acceptable because these long-generated requests are rare as shown in Fig. 6.

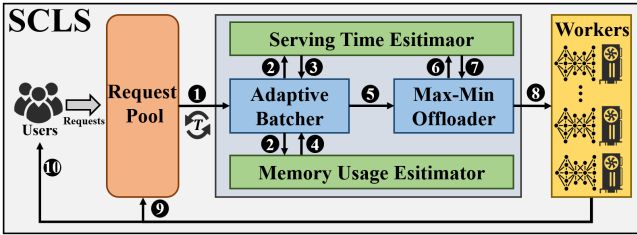


Figure 7: SCLS system overview. The arrows represent data transferred between modules, where ① is requests, ② is temporary batches, ③ and ⑦ are estimated serving time, ④ is estimated memory consumption, ⑤, ⑥, and ⑧ are batches, ⑨ is uncompleted requests, ⑩ is completed requests.

4 SOLUTION DESCRIPTION

4.1 System Overview

SCLS has four core modules, a serving time estimator, a memory usage estimator, an adaptive batcher, and a max-min offloader. The system overview of SCLS is presented in Fig. 7.

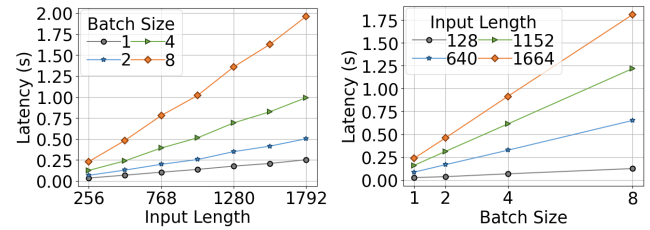
SCLS periodically fetches all requests from the request pool with a time interval T and hands them over to the adaptive batcher. The adaptive batcher leverages a dynamic programming-based algorithm to group the requests into batches with the goal of minimizing the total serving time of all batches. In each step of the batching algorithm, the adaptive batcher leverages the estimated serving time of temporarily grouped batches to update the state transfer function and utilizes estimated memory consumption to guarantee that the serving process will not cause OOM errors. After the batching procedure finishes, batches will be offloaded to workers by the max-min offloader, who schedules batches with long estimated serving time to lightly loaded workers to achieve load balancing. After workers finish batch serving, completed requests are returned to the user, and uncompleted requests are sent to the request pool to be scheduled with newly arrived requests.

A worker is an LLM instance running on a specific inference engine. The worker’s receiving thread receives the batch from the offloader and saves it in a local queue, while the worker’s processing thread continuously fetches a batch from the queue and serves it. In this paper, we implement the hf-worker and ds-worker to load and run LLM instances using hugging-face transformers and deepspeed-inference as inference engines, respectively.

4.2 Efficient Serving Time Estimation

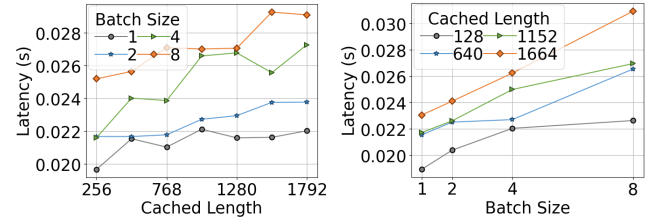
The serving time estimator estimates the batch serving time according to the batch input length, batch size, and slice length.

Existing inference engines such as huggingface-transformers and deepspeed-inference serve requests with static batching. For each batch, they pad all the batched requests to the longest input length of requests in the batch before serving. Besides, during batch serving, if a request has generated the EOS token but there are other requests that need to continue generating tokens, it will still participate in the subsequent computation and generate invalid tokens which are discarded after batch serving. Therefore, for static batching, the serving time of a batch is determined by the batch size, the batch input length, and the batch generation length.



(a) $T_{\text{prefill}}(N, L_i)$ under different input length. (b) $T_{\text{prefill}}(N, L_i)$ under different batch sizes.

Figure 8: Prefill latency under deepspeed-inference (DS).



(a) $\tau_{\text{decode}}(l, N)$ under different cached lengths. (b) $\tau_{\text{decode}}(l, N)$ under different batch sizes.

Figure 9: Per-iteration decoding latency under DS.

An intuitive way to estimate the batch serving time is to directly profile the serving time for various batch input lengths, batch generation lengths, and batch sizes. However, this is computationally expensive and requires additional profiling when the range of the predefined maximal generation length limit changes. To avoid this problem, we look at the serving procedure and model the time consumed in the prefill and decoding phases, respectively.

Given a batch \mathcal{B} whose batch size, batch input length, and batch generation length are separately represented as N , L_i , and L_o . The batch serving time is calculated by

$$T_{\text{serve}}(N, L_i, L_o) = T_{\text{prefill}}(N, L_i) + T_{\text{decode}}(N, L_i, L_o), \quad (1)$$

where $T_{\text{prefill}}(N, L_i)$, and $T_{\text{decode}}(N, L_i, L_o)$ are the serving latency in the prefill and decoding phase, respectively. Since the prefill phase computes key and value tensors for all the input tokens, the latency is determined by the batch input length L_i and the batch size N . In the decoding phase, the serving procedure runs in an iterative manner, and therefore $T_{\text{decode}}(N, L_i, L_o)$ can be calculated by summing up the latency in each decoding iteration, which is expressed by

$$T_{\text{decode}}(N, L_i, L_o) = \sum_{l=1}^{L_o} \tau_{\text{decode}}(L_i + l, N), \quad (2)$$

where $\tau_{\text{decode}}(l, N)$ denotes the serving latency in the decoding iteration. Since in each decoding iteration, for each request, only one token is fed to the LLM and extracts features from all the previously cached tokens to make a prediction, $\tau_{\text{decode}}(l, N)$ is determined by the cached length l and the batch size N .

We profile the prefill latency $T_{\text{prefill}}(N, L_i)$ of an LLaMA2-13B instance using deepspeed-inference-v0.13.3 as the inference engine under various batch sizes and batch input lengths. To clearly

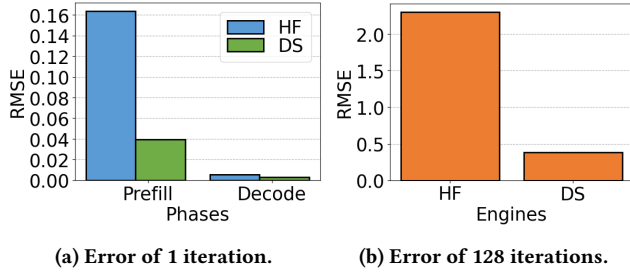


Figure 10: Serving time estimation error of various inference engines, where HF and DS are short for huggingface-transformers and deepspeed-inference, respectively.

show the individual effect of batch size N and batch input length L_i on $T_{\text{prefill}}(N, L_i)$, we plot two sub-figures with these two factors as the horizontal axis in Fig. 8. Similarly, we also profile the per-iteration latency $\tau_{\text{decode}}(l, N)$ for different cached lengths and batch sizes and show the effect of cached length l and batch size N on $\tau_{\text{decode}}(l, N)$ in Fig. 9a and Fig. 9b, respectively.

For the prefill latency $T_{\text{prefill}}(N, L_i)$, we can observe that when the batch size is fixed, $T_{\text{prefill}}(N, L_i)$ increases linearly with the increase of the batch input length L_i from Fig. 8a. Besides, as shown in Fig. 8b, when the input length is fixed, the $T_{\text{prefill}}(N, L_i)$ increases linearly with the increase of the batch size N as well. We also profile the prefill latency for huggingface-transformers, and observe the same phenomenon. Therefore, we use the following function to fit $T_{\text{prefill}}(N, L_i)$.

$$T_{\text{prefill}}(N, L_i) = p_1 \cdot N \cdot L_i + p_2 \cdot N + p_3 \cdot L_i + p_4, \quad (3)$$

where p_1, p_2, p_3 , and p_4 are parameters to be fitted. Under this function, $T_{\text{prefill}}(N, L_i)$ is a linear function of the batch input length L_i when the batch size N is fixed, and when L_i is fixed, $T_{\text{prefill}}(N, L_i)$ is also a linear function of N , which is consistent with our observations. We leverage the profiled prefill latency data of various engines to fit the function. Fig. 10a presents the fitting error metric, root-mean-square error (RMSE) which represents the average gap between the estimated and actual latency. As shown in Fig. 10a, the average gap is merely 0.16s for huggingface-transformers and less than 0.04s for deepspeed-inference, achieving an accurate estimation. Hence, Eq. (3) is used to compute the prefill latency.

For the per-iteration decoding latency $\tau_{\text{decode}}(l, N)$, we can observe from Fig. 9a that when the batch size is fixed, $\tau_{\text{decode}}(l, N)$ rises with fluctuations as the cached length increases. Besides, as shown in Fig. 9b, when the cached length is fixed, $\tau_{\text{decode}}(l, N)$ also shows a rising trend with the increase of the batch size, and when the cached length is large, the tendency tends to be linear. We also collect per-iteration decoding latency profiles for huggingface-transformers, and observe the same phenomenon. We try to estimate the per-iteration latency the same way we estimate the prefill latency using the following function.

$$\tau_{\text{decode}}(l, N) = d_1 \cdot N \cdot l + d_2 \cdot N + d_3 \cdot l + d_4, \quad (4)$$

where d_1, d_2, d_3 , and d_4 are parameters to be fitted. Fig. 10a presents the estimation error of $\tau_{\text{decode}}(l, N)$ under various inference engines, we can find that the fitting error is negligible, which confirms that the estimation is accurate.

Thus, by incorporating Eq. (4) into Eq. (2), we can obtain the estimated serving time of the decoding phase. Adding the decoding latency to the prefill latency computed by Eq. (3), we can get an estimate of the batch serving time. However, although the estimation error of a single decoding iteration is low, the error accumulates as the generation process goes on. Therefore, we evaluate the estimation error of overall batch serving time for an iteration number of 128 under various batch input lengths and batch sizes. As shown in Fig. 10b, the average error is merely 2.3s for HF and less than 0.4s for DS, which confirms that the estimation is accurate.

From Fig. 10, we can find that both the per-iteration error and multi-iteration error of HF are much higher than those of DS. This is because DS leverages customized CUDA kernels to accelerate the computation of transformer blocks, so its latency bases are much smaller than that of HF, and hence the average estimated latency error is smaller than that of HF.

SCLS sets the iteration number limit for static batching to a small slice length S , when the number of iterations reaches S , the batch serving ends regardless of whether or not all requests have generated the EOS token. Therefore, we can consider the batch generation length L_o to be S for batch serving. Hence, the serving time of SCLS can be accurately and quickly estimated by $T_{\text{serve}}(N, L_i, S)$, where N and L_i can be directly obtained before serving.

Compared with estimating the batch serving time by directly profiling the whole serving time under various batch input lengths and batch sizes for a given slice length, such a modeling approach adopted by the serving time estimator only needs to profile the prefill and decoding latency of a single iteration, which greatly reduces the computational overhead of profiling. Moreover, when the slice length changes, the serving time estimator does not need re-profiling, which achieves a flexible and efficient estimation.

If all requests in the batch generate the EOS token before the generation length reaches S , the batch serving will finish prematurely and the estimated serving time will be inaccurate. However, since S is always set small, the likelihood of the premature finish happening is small, and the performance of SCLS won't be affected. We also verify this through experiments in Section 5.

4.3 Practical Memory Usage Estimation

The memory usage estimator leverages the batch size, batch input length, and slice length to determine whether a batch of requests will cause OOM errors during batch serving.

During LLM serving, GPU memory is mainly occupied by the parameters of the LLM and the key-value cache of requests. The memory consumed by the LLM parameters is constant, but the memory consumed by the key-value cache varies with the batch size, batch input length, and batch generation length. Since for static batching, both the pad tokens and the invalid tokens generated in the request-waiting process produce key and value tensors that are cached and occupy memory, the memory consumption of the key-value cache can be calculated by

$$M_{kv}(N, L_i, L_o) = (L_i + L_o) \cdot N \cdot \Delta, \quad (5)$$

where N , L_i , L_o , and Δ respectively represent the batch size, the batch input length, the batch generation length, and the per-token memory usage of key and value tensors. Δ is determined by the model architecture.

To avoid OOM errors during serving, the memory usage of the key-value cache can not exceed the maximal available GPU memory M_{ava} , which can be calculated by

$$M_{ava} = M_{cap} - M_{model} - M_{engine}, \quad (6)$$

where M_{cap} is the GPU memory capacity, M_{model} is the memory occupied by the LLM parameters, and M_{engine} is the memory utilized by the inference engine to store engine-specific data.

Theoretically, given the batch size N , the batch input length L_i , and the slice length S , in SCLS, the memory estimator can determine whether the OOM errors will occur during batch serving by simply checking if the following constraint hold

$$M_{kv}(N, L_i, S) \leq M_{ava}. \quad (7)$$

In addition, by incorporating Eq. (5) into Eq. (7) and rearranging it, we can obtain Eq. (8), which shows that for a given input length L_i , the maximal batch size N_{max} can be smaller when the slice length is longer. Therefore, if we set the slice length S to the pre-defined maximal generation length, N_{max} will be small and SCLS degenerates into SLS. On the contrary, by setting the slice length S to a small value, more requests can be batched together to achieve a high throughput.

$$N_{max} = \lfloor \frac{M_{ava}}{\Delta \cdot (L_i + S)} \rfloor. \quad (8)$$

In practice, for the same model and batched requests, there is a gap between the actual GPU memory usage and the theoretical memory usage for different inference engines due to the engine-specific memory management mechanism.

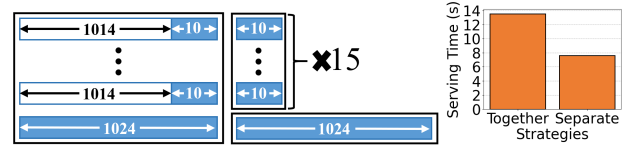
Huggingface-transformers (HF), as an inference engine based entirely on pytorch [19], produces memory fragmentation that cannot be utilized during the batch serving. Therefore, for HF, it is necessary to multiply M_{ava} in Eq. (7) by an additional coefficient ζ less than 1, and the constraint is rewritten as

$$M_{kv}(N, L_i, S) \leq \zeta \cdot M_{ava}. \quad (9)$$

Deepspeed-inference (DS) has an inflexible memory management mechanism. Although it can serve batched requests with a larger batch size when the batch input and generation lengths are shorter, we experimentally find that it is unable to determine whether OOM errors will occur using Eq. (9), even if ζ is set to a small value such as 0.6. Therefore, for DS, under a given slice length S , we profile the maximal batch size for various batch input lengths and make rules for determining whether OOM will occur during batch serving.

4.4 Serving Time-Oriented Batching

As shown in Fig. 11, under a slice length of 128, given 15 requests with an input length of 10 and 1 request with an input length of 1024, if they are batched together, it takes 13.5s to finish serving for an LLaMA2-13B instance deployed with huggingface-transformers-v4.35.0. If the requests with input lengths of 10 and 1024 are divided into two separate batches, the total serving time is only 7.6s, which is far less than the serving time of batching them together. This is because all the requests are padded to 1024 tokens when they are batched together, which greatly increases the per-iteration prefill and decoding latency for the requests with an input length of 10.



(a) Together batching. (b) Separate batching. (c) Serving time.

Figure 11: Batching example. Under a given slice length of 128, various batching strategies have a large difference in the serving time. In sub-figure (a), white and blue grids represent pad and input tokens, respectively.

Accordingly, we propose the adaptive batcher which leverages a dynamic programming-based algorithm to partition requests into batches with the goal of minimizing the total batch serving time. By aiming to reduce serving time, the algorithm can make an excellent trade-off between mitigating padding and increasing batch size.

Pseudocode of the batching algorithm is presented in Algorithm 1. The batching algorithm first sorts requests in ascending order by their input lengths. Then the state array \mathcal{T} is created, where $\mathcal{T}[i]$ denotes the minimal total batch serving time for the first i requests. The initial state $\mathcal{T}[0] = 0$ indicates that the total serving time is 0 when there is no request to batch. The position array \mathcal{P} stores positions for partitioning requests into batches.

During dynamic programming, the algorithm sequentially traverses each request. For each request, the algorithm first treats it as

Algorithm 1: Serving Time-Oriented Batching

```

Input:  $\mathcal{R}$ : a list of requests;  $S$ : the slice length
Output:  $\mathcal{L}$ : a list of batches
1 Sort  $\mathcal{R}$  by the request input length in ascending order
2  $n \leftarrow$  the number of requests in  $\mathcal{R}$ 
   // States denoting the total serving time
3  $\mathcal{T} \leftarrow$  array of zeroes[0..n]
   // Positions for splitting batches
4  $\mathcal{P} \leftarrow$  array of zeroes[0..n]
5 for  $i \leftarrow 1$  to  $n$  do
6    $\mathcal{P}[i] \leftarrow i - 1$  // Separate a request into a batch
7    $L_i \leftarrow$  input length of the request  $\mathcal{R}[i - 1]$ 
8    $\mathcal{T}[i] \leftarrow \mathcal{T}[i - 1] + T_{serve}(1, L_i, S)$ 
9    $j \leftarrow i - 1$ 
10  while  $j > 0$  and not OOM( $i - j + 1, L_i, S$ ) do
11     $t \leftarrow \mathcal{T}[j - 1] + T_{serve}(i - j + 1, L_i, S)$ 
12    if  $t < \mathcal{T}[i]$  then
13       $\mathcal{T}[i] \leftarrow t$  // Update total serving time
14       $\mathcal{P}[i] \leftarrow j - 1$  // Record splitting position
15     $j \leftarrow j - 1$ 
16  $\mathcal{L} \leftarrow$  empty list // Currently,  $i$  is equal to  $n$ 
17 while  $i > 0$  do
18    $p \leftarrow \mathcal{P}[i]$ 
19   Batch  $\mathcal{R}[p : i]$  together and append the batch to  $\mathcal{L}$ 
20    $i \leftarrow p$ 
21 return  $\mathcal{L}$ 

```

a separate batch, and then tries to batch it together with preceding requests to minimize the total batch serving time while guaranteeing that OOM errors will not occur. The state transfer function of dynamic programming is expressed by

$$\mathcal{T}[i] = \min_{0 < j \leq i} (\mathcal{T}[j-1] + T_{serve}(i-j+1, L_i, S)), \quad (10)$$

where $i - j + 1$ computes the batch size. Since requests are sorted by the request input length at the beginning, when traversing to the i th request, its input length is the maximal input length of the first i requests, and hence its input length can be utilized as the batch input length L_i to calculate the estimated batch serving time T_{serve} . After the dynamic programming, the requests are divided into batches according to the recorded splitting positions.

In the batching algorithm, whether OOM errors will occur is determined by the memory usage estimator, and the estimated serving time of batches is calculated by the serving time estimator.

4.5 Balanced Load-Oriented Offloading

The offloader achieves load balancing among multiple workers using a max-min-based algorithm. The load of a worker is defined as the time it takes to serve all the batches in its local queue and the initial load of each worker is 0.

The offloader offloads batches to workers one by one. At each offload, it schedules the batch with the longest estimated serving time to the worker with minimal load and then updates the worker's load with

$$T_{load}(w) \leftarrow T_{load}(w) + T_{serve}(N, L_i, S), \quad (11)$$

where $T_{load}(w)$ represents the load of the least loaded worker w and $T_{serve}(N, L_i, S)$ denotes the estimated serving time of the batch to be offloaded, where N , L_i , and S are the batch size, batch input length, and slice length, respectively.

In addition, after each time a worker completes batch serving, SCLS updates the load of the worker by subtracting the estimated serving time of the batch it just served from its load. This can prevent the estimation error of serving time from accumulating in the load, thus enhancing the load-balancing.

4.6 Adaptive Schedule Interval Update

SCLS periodically fetches requests from the request pool and hands them over to the adaptive batcher at a time interval of T . After each batch offloading, SCLS updates the time interval T by

$$T \leftarrow \max(\lambda \cdot \min_w(T_{load}(w)), \Gamma), \quad (12)$$

where Γ is a pre-defined minimal time interval, $T_{load}(w)$ is the load of worker w , and λ is a factor less than 1.

Accordingly, when the load of each worker is light, T decreases, so that requests can be processed by workers in time without waiting for a long time in the request pool, thus reducing the request response time. When there are a lot of batches waiting in the local queue of each worker, T increases so that the adaptive batcher is highly likely to batch more requests together, thus increasing the throughput. Due to the serving time estimation error, λ is introduced to prevent workers from being idle when the load is overestimated, and Γ is introduced to avoid feeding too few requests to the adaptive batcher when the load is under-estimated.

Algorithm 2: DeepSpeed-Inference OOM Judgment

Input: L_i :batch input length; S : slice length; N : batch size
Output: An expression that OOM will occur if true
1 $L \leftarrow L_i + S // L \leq 2048$ under experimental settings
2 **if** $L > 1024$ **then**
3 **return** $N > 12$
4 **else if** $L > 512$ **then**
5 **return** $N > 22$
6 **else**
7 **return** $N > 28 //$ Total token number $L \leq 512$

5 EXPERIMENTAL EVALUATION

5.1 Experiment Setup

Testbed. Experiments are conducted on our testbed equipped with 8 NVIDIA A100 80GB GPUs connected over NVLink, 800GB CPU memory, and two 2.90GHz 32-core Intel(R) Xeon(R) CPUs.

Settings. We set both the maximal raw request input length and the maximal generation length limit to 1024. When the raw input length of a request is greater than 1024, it is truncated to 1024. When the total number of generated tokens of a request is greater than 1024, the request is returned.

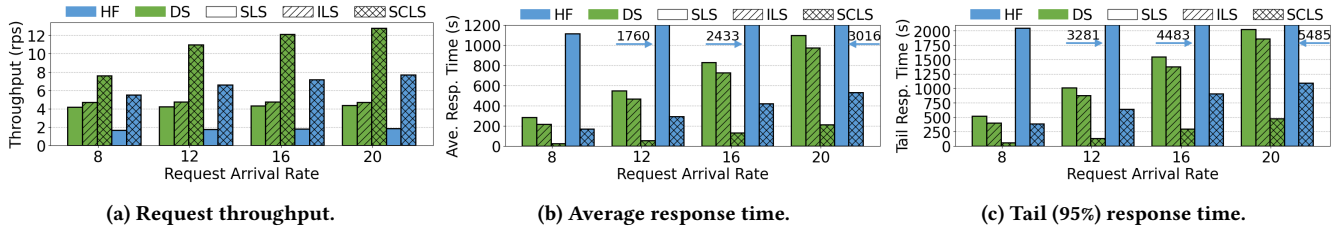
Implementation. We implement SCLS and workers for hugging-face transformers (HF) v4.35.0 and deepspeed inference (DS) v0.13.3 using Python 3.8. For the serving time estimator, we use `curve_fit` function from the `scipy` library [20] to fit Eq. (3) and Eq. (4) with profiled per-iteration latency data. The memory estimator leverages different methods for the two inference engines to judge whether OOM will occur. For HF, Eq. (9) is used where ζ is set to 0.9. For DS, under the experimental settings, it determines if OOM errors will occur by rules that are presented in Algorithm 2. To fetch more requests while keeping workers busy, SCLS dynamically adjusts the schedule time interval T by Eq. (12), where λ is set to 0.5, Γ is set to 6s and 3s for HF and DS according to their inference speed, respectively. Moreover, the slice length is set to 128 if not specified.

Workflow. We deploy 8 LLaMA2-13B workers on 8 NVIDIA A100 80GB GPUs. After LLM instances are loaded, we send requests from the CodeFuse request trace in the order they actually arrived. Requests are sent for 10 minutes and the request arrival times are generated using Poisson distribution with various request rates.

Metrics. We use request throughput, average response time, and 95% tail response time as evaluation metrics, where the response time is the total time between the user sending the request and receiving the generated results.

Baselines. We compare SCLS with SLS and ILS schedulers. Since HF only supports static batching, when using HF as the inference engine, we only compare SCLS with SLS. For DS, we not only compare SCLS with SLS but also use DeepSpeed-Fastgen, an ILS scheduler implemented on top of DS, to compare with SCLS.

- **Sequence-level Scheduling (SLS)** [2, 3]: The scheduler offloads requests to workers using the round-robin policy. Workers serve received requests in an FCFS manner with a fixed batch size. Since different engines have various M_{engine} , for HF and DS workers, the fixed batch size is set to 16 and 12 to avoid OOM errors, respectively.

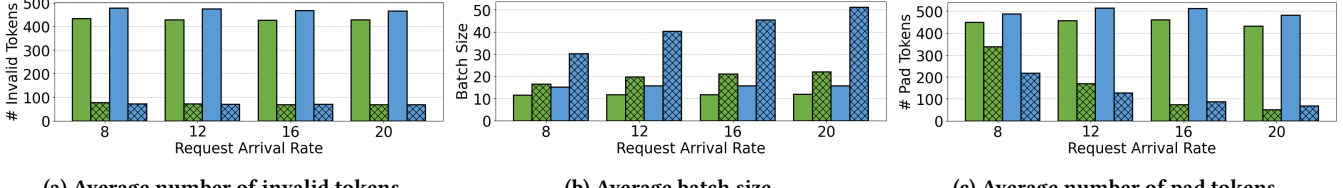


(a) Request throughput.

(b) Average response time.

(c) Tail (95%) response time.

Figure 12: Request throughput, average response time and tail response time under various arrival rates.



(a) Average number of invalid tokens.

(b) Average batch size.

(c) Average number of pad tokens.

Figure 13: Dive into the superiority of SCLS.

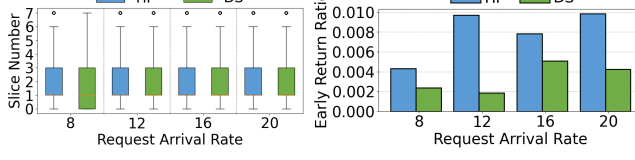


Figure 14: Dive into the overhead of SCLS.

- **Iteration-level Scheduling (ILS)** [6]: Deepspeed-FastGen, the ILS scheduler built on top of DS, is one of the state-of-the-art ILS schedulers. It achieves a low latency with continuous batching and split-fuse technologies. However, it utilizes the round-robin policy to offload requests and adopts a conservative memory management mechanism which limits the throughput. For DS, we take FastGen-v0.2.0 as the ILS scheduler to compare with SCLS.

5.2 Overall Performance

In this subsection, we compare the performance of SCLS to the baseline scheduling techniques under different request arrival rates.

The experimental results are depicted in Fig. 12, where *different colors represent different inference engines, and various hatch styles represent various scheduling techniques*. We can see that SCLS always outperforms SLS and ILS and shows the best performance when integrating with various inference engines under different request arrival rates.

Compared with SLS, the superiority of SCLS mainly comes from three sources. The first is to return completed requests in time, thus avoiding request waiting and greatly reducing the number of generated invalid tokens. The second is to serve requests with a large batch size to achieve a high throughput. The third is to reduce the serving latency by mitigating the padding overhead using the adaptive batcher. Due to the different memory management mechanisms of HF and DS, the maximal batch size that can be supported under the same batch input length and the same slice length is

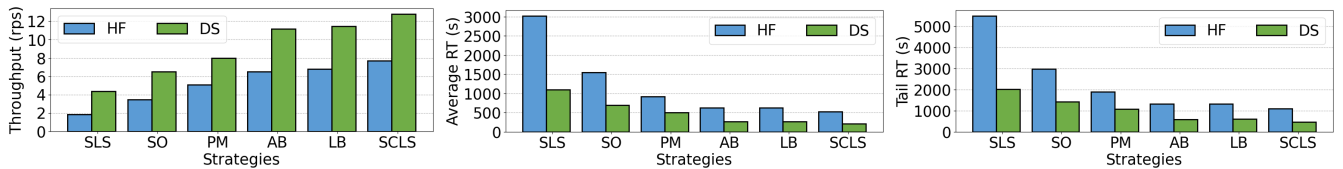
different, and SCLS can obtain different performance gains when integrated with various inference engines.

HF can flexibly support variable batch sizes. Given the request input length and the slice length, SCLS’s adaptive batcher can batch more requests together to achieve a larger batch size when using HF as the inference engine. As shown in Fig. 12, SCLS can increase the throughput by 232.3% to 315.8%, decrease the average response time by 82.4% to 84.9%, and decrease the tail response time by 79.8% to 81.0% compared with SLS when integrated with HF.

DS’s memory management mechanism is not flexible enough to support variable batch sizes, and hence we use the conservative rules presented in Algorithm 2 to prevent OOM errors. Therefore, when SCLS is integrated with DS, the throughput is only increased by 82.5% to 191.9% compared with SLS, which is less than the gain when integrated with HF. However, due to the timely return of requests and low padding overhead, SCLS can still reduce the average response time by 80.8% to 91.1% and the tail response time by 76.6% to 88.9% compared with SLS when integrated with DS.

Compared with ILS, SCLS can support larger batch sizes without causing OOM errors, whereas Deepspeed-FastGen adopts a conservative memory management policy to prevent OOM and speedup inference by limiting the number of parallel-processing requests. As a result, SCLS can improve the throughput by 61.6% to 171.0%, reduce the average request response time by 78.4% to 88.3%, and reduce the tail response time by 74.6% to 85.8% compared with ILS when integrated with DS.

To dive into the superior performance of SCLS, we present the average invalid token number of requests, the average batch size, and the average pad token number of requests for SLS and SCLS at various request rates when integrated with various inference engines in Fig. 13. For SCLS, if a request is rescheduled multiple times, we add up the number of pad tokens at each schedule as its pad token number. From Fig. 13a, we can see that under SCLS, the number of invalid tokens generated in the request waiting process is greatly reduced, which implies that the completed request can be returned in time through generation slicing. Besides, we can also find that the batch size is greatly improved from Fig. 13b. The improvement is

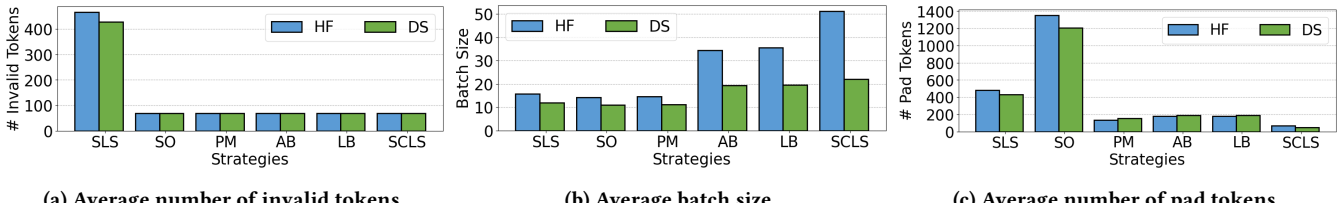


(a) Request throughput.

(b) Average response time (RT).

(c) Tail (95%) response time (RT).

Figure 15: Request throughput, average response time and tail response time under various strategies.



(a) Average number of invalid tokens.

(b) Average batch size.

(c) Average number of pad tokens.

Figure 16: Dive into the results of ablation experiments.

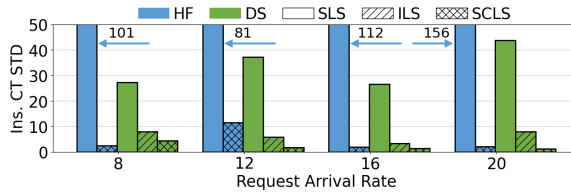


Figure 17: Load imbalance under various request rates

more significant when SCLS is integrated with HF, which is 100.3% to 226.1%. For DS, the batch size improvement of SCLS over SLS is only 43.2% to 86.1%, which is not as much as integration with HF due to the inflexible memory management mechanism of DS. Moreover, as the request rate increases, more requests of varying input and generation lengths are sent to the adaptive batcher, which provides more opportunities for the batching algorithm to batch more requests together and reduce the computational overhead of pad tokens. Thus, from Fig. 13b and Fig. 13c, we can see that under SCLS, the batch size increases with the request rate while the number of pad tokens decreases with the request rate.

The overhead of SCLS comes from the re-computation of the prefill phase with each reschedule. We illustrate the distribution of request reschedule number (a.k.a. slice number) under different request rates in Fig. 14a. We find that the vast majority of requests have less than three reschedules, this is because their request generation lengths are small and can complete generation within three slices. Although the total serving time of requests with long generation lengths is increased due to multiple re-computations of the prefill phase, they also benefit from SCLS as their queuing time is greatly reduced due to increased throughput.

In Section 4.2, we mentioned that if all requests generate EOS before the generation length reaches the slice length, the requests will be returned early, which leads to inaccurate time estimation. To verify that this happens very rarely, in Fig. 14b, we calculate the proportion of these early returned batches to the total number of served batches. We can find that early return happens rarely, with a maximal proportion less than 1%, and hence the early return has negligible effect on the performance of SCLS.

5.3 Load Balance

We calculated the standard deviation (STD) of each instance's completion time (CT) at the end of the experiment in Fig. 17.

We find that the standard deviation of SCLS is always the smallest, which indicates that the completion time of each instance is similar and SCLS achieves load balancing across multiple LLM instances. This is because the offloading algorithm can accurately estimate the load of workers and leverage the max-min algorithm to reduce the load gap between workers.

Without knowing the request generation length, SLS and ILS leverage the round-robin policy to offload requests, which may schedule requests with long generation lengths and requests with short generation lengths to different instances in a period of time. Such an unbalanced workload accumulates over time and leads to different instance completion times, Therefore, they have a higher standard deviation of instance completion time than SCLS.

5.4 Ablation Studies

In this section, we validate the performance gain of the design features of SCLS. We keep adding features to SLS to constitute multiple strategies and then verify their performance in terms of request throughput and response time at a request arrival rate of 20. The experimental results are presented in Fig. 15.

Slice-Only (SO) limits the number of iterations for static batching to the slice length, returning completed requests in time, and re-send unfinished requests to workers. It offloads requests to workers using the round-robin policy. Workers serve received requests in an FCFS manner with a fixed batch size. **Padding-Mitigating (PM)** implements an incomplete batching algorithm on top of SO, where the batch size is limited to 12 and 16 for DS and HF, respectively. Besides, PM fetches requests from the request pool at the fixed time interval Γ and offloads batches to workers with the round-robin policy as well. **Adaptive-Batching (AB)** lifts the fixed batch size limitation on the basis of PM and implements the complete serving time-oriented batching algorithm. **Load-Balancing (LB)** adds the max-min offloading policy to AB to achieve a balanced workload across multiple LLM instances. By integrating the adaptive batch schedule update mechanism on LB, SCLS is constructed.

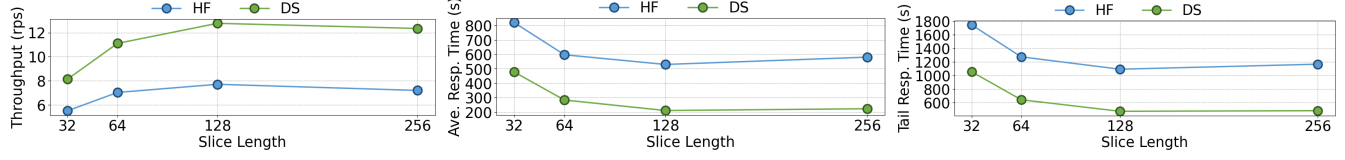


Figure 18: Request throughput, average response time and tail response time under various slice lengths.

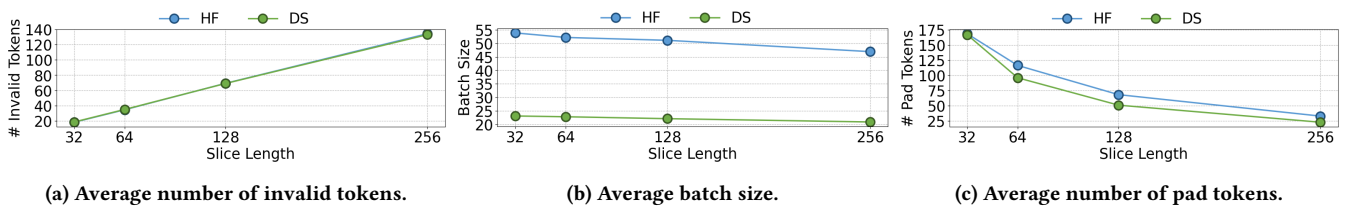


Figure 19: Dive into the slice length impact on SCLS performance .

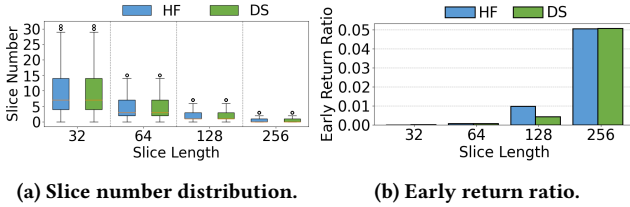


Figure 20: Dive into the slice length impact on SCLS overhead.

As shown in Fig. 15, the performance of strategies gradually enhances as more features are integrated, where the throughput increases and the response time decreases. Compared with SLS, SO is able to return completed requests timely, thus gaining a performance boost. Compared with SO, PM continues to improve performance by reducing the additional computational overhead caused by pad tokens using the incomplete batching algorithm. Compared with PM, AB increases the batch size to improve throughput as shown in Fig.16b. LB achieves a balanced load across workers, thus preventing workers from being idle and fully utilizing workers' computing capability to further improve the throughput. The adaptive schedule interval update mechanism allows more requests to be fetched when the workload is heavy, giving the batching algorithm more chances to increase the batch size and reduce pad tokens.

We also present the average invalid token number of requests, the average batch size, and the average pad token number of requests for these strategies in Fig. 16. We can see that generation slicing can significantly reduce invalid tokens, and the batching algorithm can greatly reduce pad tokens and increase the batch size. Although the number of pad tokens of AB and LB is slightly higher than that of PM, the performance of AB and LB is higher than that of PM due to the great increase in batch size, which confirms that by aiming to reduce serving time, the batching algorithm can make an excellent trade-off between mitigating padding and increasing batch size.

5.5 Impact of Slice Length

In this section, we explore the impact of slice length on the performance of SCLS. We evaluate the performance of SCLS at a request rate of 20 under various slice lengths. The experimental results are

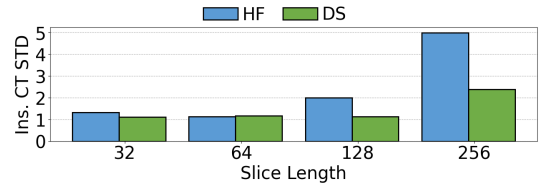
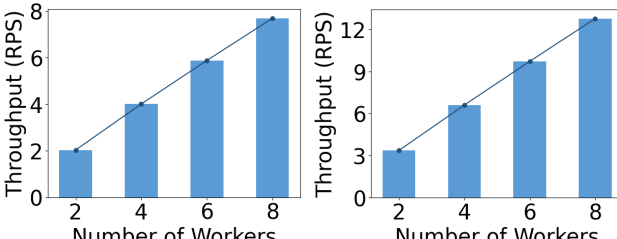


Figure 21: Load imbalance under various slice lengths

shown in Fig. 18. Besides, we also present the average invalid token number of requests, the average batch size, and the average pad token number of requests in Fig. 19. Mover, we also depict the slice number distribution and early return ratio in Fig. 20 to analyze how the overhead varies with the slice length.

From Fig. 18, we can find that with the increase in slice length, the performance first increases and then decreases. This is because when the slice length is set too small, there are a lot of reschedules of requests. The reschedules cause requests to be padded multiple times and hence the computational overhead caused by padding is severe when the slice length is set small as shown in Fig. 19c. Besides, the frequent reschedules cause a large number of prefill re-computations. Although with a small slice length, completed requests can be returned in a timely manner and the batch size can be relatively large, it is not enough to make up for the computational overhead of the large amount of re-padding and prefill re-computations. When the slice length is increased, although the batch size decreases slightly, the number of reschedules decreases dramatically as shown in Fig. 20a, and hence the performance is improved. However, setting the slice length too long not only further decreases the batch size as shown in Fig. 19b, but also causes more serious request waiting, and more invalid tokens are generated as shown in Fig.19a, so the performance decreases. Furthermore, a long slice length causes a large early return ratio as shown in Fig. 20b, which makes the serving time estimation inaccurate, and hence the workload becomes unbalanced as shown in Fig. 21. Therefore, when setting the slice length, we need to do a trade-off between the request padding, the batch size, the prefill re-computations, and the request waiting.



(a) Huggingface-Transformers. (b) DeepSpeed-Inference.

Figure 22: Scalability of SCLS.

5.6 Scalability

We evaluate the throughput of SCLS under different numbers of workers at a request arrival rate of 20, where each worker is deployed on an NVIDIA A100 80GB GPU. The experimental results are shown in Fig. 22. We can see that the throughput grows linearly with the number of workers, which confirms the scalability of SCLS.

6 RELATED WORKS

Model compression. Quantization [21–25] reduces the numerical precision of model weights to lower-bit representations to reduce the memory consumed by model parameters. Knowledge distillation [26–30] trains small-scale student models using outputs of large teacher models to compress the model size while maintaining prediction accuracy. Pruning [31–33] removes redundant network modules from LLMs and improves the inference speed. These works are orthogonal to SCLS, and the computational efficiency of SCLS can be further enhanced with compressed LLMs.

Speculative decoding. Speculative decoding [34–37] leverages a small language model to autoregressively generate draft outputs and refine the draft with the large model periodically. However, the increase in serving efficiency of speculative decoding depends on the predictive power of the small model. Besides, most speculative decoding algorithms do not support batch processing and are not applicable to high-concurrency scenarios.

Request scheduling. Existing serving systems [2, 3] lack model-specific optimizations and adopt the sequence-level scheduling to serve requests in an FCFS manner with a fixed batch size which leads to severe computational inefficiency for LLM serving. Orca [4] and FastGen [6] leverage the iteration-level scheduling to improve the serving efficiency but they adopt conservative memory management strategies which limit the throughput. On the shoulder of the aforementioned works, PiA [38] and S^3 [39] propose to roughly predict the request generation length to enhance serving efficiency for sequence-level and iteration-level scheduling, respectively. However, they require significant computational overhead to fine-tune LLMs or train predictors while SCLS can support LLMs seamlessly without any additional computational overhead.

Low-level optimization. Kernel optimization [5, 16, 40, 41] speeds up training and inference by implementing efficient CUDA kernels for transformer-based LLMs to improve computational efficiency. Parallelism optimization [42–46] proposes to split the model at intra-layer and inter-layer granularity to enable distributed training and inference for LLMs. These studies are orthogonal to SCLS, and SCLS can be augmented with these low-level techniques.

DNN serving system. Recently proposed deep neural network (DNN) serving systems [47–49] serve requests in a model-less manner, where developers simply specify the performance and accuracy requirements for their applications, and the serving system chooses a model for each query. Besides, [50–52] propose to leverage the automated resource management of serverless platforms to elastically handle requests. Moreover, Alpserve [53] improves the serving efficiency with statistical multiplexing. However, none of these systems are specifically optimized for generative LLMs.

7 DISCUSSION

Integration with continuous batching. For continuous batching, if the generation length of a request is too long, it will consume a large amount of memory, which causes newly arrived requests to queue up and can not be added to the serving process due to insufficient memory. By limiting the number of generated tokens for requests in each schedule to a small slice length, we can solve this problem by timely rescheduling the long request to an instance with more free memory. Besides, we can also accurately estimate the memory consumed by requests in each schedule to serve as many requests in parallel as possible without causing OOM errors and achieve balanced memory consumption across multiple LLM instances. We are working on implementing SCLS on top of vllm [54] to integrate with continuous batching, and we are also trying to mitigate the overhead of the prefill re-computation by proactively swapping the key-value cache between the CPU and GPU memory.

Fast support for inference engines. SCLS is a pure scheduling system. It can quickly support any inference engine that can serve requests with static batching without any modification of the engine. In this paper, we support huggingface-transformers and deepspeed-inference with only 350 lines of code, and we are making efforts to support more inference engines such as tensorrt-llm [55].

Seamless support for LLMs. SCLS can be directly applied to all the transformer-based LLMs that generate tokens in an autoregressive manner, and SCLS does not require additional program development to support new models. Besides, no matter what engines the LLMs are loaded and run on, SCLS takes effect as long as those engines use the key-value cache mechanism during inference.

8 CONCLUSION

In this paper, we propose SCLS, a pure scheduling system to improve throughput for LLM serving and achieve load balancing across multiple LLM instances. We introduce the technical details of SCLS integration with static batching in this paper, where the number of iterations for each batch serving is limited to a small slice length. In this way, SCLS can obtain an accurate estimation of memory consumption and batch serving time, which enables effective scheduling. Since in actual scenarios the majority of requests have small generation lengths, the prefill re-computation overhead of SCLS is small when the slice length is set to an appropriate value. Extensive experiments are conducted to demonstrate that SCLS can far outperform existing ILS and SLS schedulers in terms of request throughput while greatly alleviating load imbalance. In the future, we will implement efficient CUDA kernels to achieve dedicated GPU memory management strategies for SCLS to further improve batch serving efficiency.

REFERENCES

[1] Codefuse. <https://codefuse.alipay.com>, 2024.

[2] Triton inference server. <https://github.com/triton-inference-server/server>, 2023.

[3] Tensorflow serving. <https://github.com/tensorflow/serving>, 2023.

[4] Gyeong-In Yu, Joo Seong Jeong, Geon-Woo Kim, et al. Orca: A distributed serving system for transformer-based generative models. In *16th USENIX Symposium on Operating Systems Design and Implementation (OSDI 22)*, pages 521–538, 2022.

[5] Woosuk Kwon, Zuhuan Li, Siyuan Zhuang, et al. Efficient memory management for large language model serving with paginated attention. In *Proceedings of the 29th Symposium on Operating Systems Principles*, pages 611–626, 2023.

[6] Deepspeed-fastgen. <https://github.com/microsoft/DeepSpeed-MII>, 2024.

[7] Bozidar Radunovic and Jean-Yves Le Boudec. A unified framework for max-min and min-max fairness with applications. *IEEE/ACM Transactions on networking*, 15(5):1073–1083, 2007.

[8] Tom Brown, Benjamin Mann, Nick Ryder, et al. Language models are few-shot learners. *Advances in neural information processing systems*, 33:1877–1901, 2020.

[9] Hugo Touvron, Thibaut Lavril, Gautier Izacard, et al. Llama: Open and efficient foundation language models. 2023.

[10] Hugo Touvron, Louis Martin, Kevin Stone, et al. Llama 2: Open foundation and fine-tuned chat models. 2023.

[11] Zhengxiao Du, Yujie Qian, Xiao Liu, et al. Glm: General language model pre-training with autoregressive blank infilling. In *Proceedings of the 60th Annual Meeting of the Association for Computational Linguistics (Volume 1: Long Papers)*, pages 320–335, 2022.

[12] Jinze Bai, Shuai Bai, Yunfei Chu, et al. Qwen technical report. 2023.

[13] Aohan Zeng, Xiao Liu, Zhengxiao Du, et al. Glm-130b: An open bilingual pre-trained model. In *The Eleventh International Conference on Learning Representations*, 2022.

[14] Ashish Vaswani, Noam Shazeer, Niki Parmar, et al. Attention is all you need. *Advances in neural information processing systems*, 30, 2017.

[15] Thomas Wolf, Lysandre Debut, Victor Sanh, et al. Transformers: State-of-the-art natural language processing. In *Proceedings of the 2020 conference on empirical methods in natural language processing: system demonstrations*, pages 38–45, 2020.

[16] Reza Yazdani Aminabadi, Samyam Rajbhandari, Ammar Ahmad Awan, et al. Deepspeed-inference: enabling efficient inference of transformer models at unprecedented scale. In *SC22: International Conference for High Performance Computing, Networking, Storage and Analysis*, pages 1–15. IEEE, 2022.

[17] Sharegpt. <https://sharegpt.com>, 2024.

[18] Chatgpt. <https://chat.openai.com>, 2024.

[19] Adam Paszke, Sam Gross, Francisco Massa, et al. Pytorch: An imperative style, high-performance deep learning library. *Advances in neural information processing systems*, 32, 2019.

[20] P Virtanen, R Gommers, TE Oliphant, et al. Fundamental algorithms for scientific computing in python and scipy 1.0 contributors. *scipy 1.0. Nat. Methods*, 17:261–272, 2020.

[21] Elias Frantar, Saleh Ashkboos, Torsten Hoefer, and Dan Alistarh. OPTQ: Accurate quantization for generative pre-trained transformers. In *The Eleventh International Conference on Learning Representations*, 2023.

[22] Guangxuan Xiao, Ji Lin, Mickael Seznec, et al. Smoothquant: Accurate and efficient post-training quantization for large language models. In *International Conference on Machine Learning*, pages 38087–38099. PMLR, 2023.

[23] Tim Dettmers, Mike Lewis, Younes Belkada, and Luke Zettlemoyer. Gpt3. int8 (): 8-bit matrix multiplication for transformers at scale. *Advances in Neural Information Processing Systems*, 35:30318–30332, 2022.

[24] Wenqi Shao, Mengzhao Chen, Zhaoyang Zhang, et al. Omnipquant: Omnidirectionally calibrated quantization for large language models. In *The Twelfth International Conference on Learning Representations*, 2023.

[25] Jerry Chee, Yaohui Cai, Volodymyr Kuleshov, et al. Quip: 2-bit quantization of large language models with guarantees. *Advances in Neural Information Processing Systems*, 36, 2024.

[26] Kevin Li Jiang, Weituo Hao, Dinghan Shen, et al. Mixkd: Towards efficient distillation of large-scale language models. In *International Conference on Learning Representations*, 2020.

[27] Lei Li, Yankai Lin, Shuhuai Ren, et al. Dynamic knowledge distillation for pre-trained language models. In *Proceedings of the 2021 Conference on Empirical Methods in Natural Language Processing*, pages 379–389, 2021.

[28] Chang Liu, Chongyang Tao, Jiazhuan Feng, and Dongyan Zhao. Multi-granularity structural knowledge distillation for language model compression. In *Proceedings of the 60th Annual Meeting of the Association for Computational Linguistics (Volume 1: Long Papers)*, pages 1001–1011, 2022.

[29] Deyao Zhu, Jun Chen, Xiaoqian Shen, et al. Minigpt-4: Enhancing vision-language understanding with advanced large language models. In *The Twelfth International Conference on Learning Representations*, 2023.

[30] Can Xu, Qingfeng Sun, Kai Zheng, et al. WizardLM: Empowering large pre-trained language models to follow complex instructions. In *The Twelfth International Conference on Learning Representations*, 2024.

[31] Runxin Xu, Fuli Luo, and Chengyuan others Wang. From dense to sparse: Contrastive pruning for better pre-trained language model compression. In *Proceedings of the AAAI Conference on Artificial Intelligence*, volume 36, pages 11547–11555, 2022.

[32] Mingjie Sun, Zhuang Liu, Anna Bair, and J Zico Kolter. A simple and effective pruning approach for large language models. In *The Twelfth International Conference on Learning Representations*, 2023.

[33] Zichang Liu, Jue Wang, Tri Dao, et al. Deja vu: Contextual sparsity for efficient llms at inference time. In *International Conference on Machine Learning*, pages 22137–22176. PMLR, 2023.

[34] Yaniv Leviathan, Matai Kalman, and Yossi Matias. Fast inference from transformers via speculative decoding. In *International Conference on Machine Learning*, pages 19274–19286. PMLR, 2023.

[35] Heming Xia, Tao Ge, Peiyi Wang, et al. Speculative decoding: Exploiting speculative execution for accelerating seq2seq generation. In *Findings of the Association for Computational Linguistics: EMNLP 2023*, pages 3909–3925, 2023.

[36] Ziteng Sun, Ananda Theertha Suresh, Jae Hun Ro, et al. Spectr: Fast speculative decoding via optimal transport. *Advances in Neural Information Processing Systems*, 36, 2024.

[37] Sehoon Kim, Karttikeya Mangalam, Suhong Moon, et al. Speculative decoding with big little decoder. *Advances in Neural Information Processing Systems*, 36, 2024.

[38] Zangwei Zheng, Xiaozhe Ren, Fuzhao Xue, et al. Response length perception and sequence scheduling: An llm-empowered llm inference pipeline. *Advances in Neural Information Processing Systems*, 36, 2024.

[39] Yunho Jin, Chun-Feng Wu, David Brooks, and Gu-Yeon Wei. s^3 : Increasing gpu utilization during generative inference for higher throughput. *Advances in Neural Information Processing Systems*, 36, 2024.

[40] Tri Dao, Dan Fu, Stefano Ermon, et al. Flashattention: Fast and memory-efficient exact attention with io-awareness. *Advances in Neural Information Processing Systems*, 35:16344–16359, 2022.

[41] Tri Dao. Flashattention-2: Faster attention with better parallelism and work partitioning. In *The Twelfth International Conference on Learning Representations*, 2023.

[42] Yanping Huang, Youlong Cheng, Ankur Bapna, et al. Gpipe: Efficient training of giant neural networks using pipeline parallelism. *Advances in neural information processing systems*, 32, 2019.

[43] Deepak Narayanan, Aaron Harlap, Amar Phanishayee, et al. Pipedream: generalized pipeline parallelism for dnn training. In *Proceedings of the 27th ACM symposium on operating systems principles*, pages 1–15, 2019.

[44] Deepak Narayanan, Mohammad Shoeybi, Jared Casper, et al. Efficient large-scale language model training on gpu clusters using megatron-lm. In *Proceedings of the International Conference for High Performance Computing, Networking, Storage and Analysis*, pages 1–15, 2021.

[45] Xupeng Miao, Yujie Wang, Youhe Jiang, et al. Galvatron: Efficient transformer training over multiple gpus using automatic parallelism. *Proceedings of the VLDB Endowment*, 16(3):470–479, 2022.

[46] Xupeng Miao, Yining Shi, Zhi Yang, Bin Cui, and Zhihai Jia. Sdpipe: A semi-decentralized framework for heterogeneity-aware pipeline-parallel training. *Proceedings of the VLDB Endowment*, 16(9):2354–2363, 2023.

[47] Francisco Romero, Qian Li, Neeraja J Yadwadkar, and Christos Kozyrakis. {INFAAS}: Automated model-less inference serving. In *2021 USENIX Annual Technical Conference (USENIX ATC 21)*, pages 397–411, 2021.

[48] Jashwanth Raj Ganasekaran, Cyan Subhra Mishra, Prashanth Thinakaran, et al. Cocktail: A multidimensional optimization for model serving in cloud. In *19th USENIX Symposium on Networked Systems Design and Implementation (NSDI 22)*, pages 1041–1057, 2022.

[49] Yiding Wang, Kai Chen, Haisheng Tan, and Kun Guo. Tabi: An efficient multi-level inference system for large language models. In *Proceedings of the Eighteenth European Conference on Computer Systems*, pages 233–248, 2023.

[50] Ahsan Ali, Riccardo Pincioli, Feng Yan, and Evgenia Smirni. Batch: Machine learning inference serving on serverless platforms with adaptive batching. In *SC20: International Conference for High Performance Computing, Networking, Storage and Analysis*, pages 1–15. IEEE, 2020.

[51] Ahsan Ali, Riccardo Pincioli, Feng Yan, and Evgenia Smirni. Optimizing inference serving on serverless platforms. *Proceedings of the VLDB Endowment*, 15(10), 2022.

[52] Yuncheng Wu, Tien Tuan Anh Dinh, Guoyu Hu, et al. Serverless data science— are we there yet? a case study of model serving. In *Proceedings of the 2022 International Conference on Management of Data*, pages 1866–1875, 2022.

[53] Zuhuan Li, Lianmin Zheng, Yinmin Zhong, et al. {AlpaServe}: Statistical multiplexing with model parallelism for deep learning serving. In *17th USENIX Symposium on Operating Systems Design and Implementation (OSDI 23)*, pages 663–679, 2023.

[54] vllm. <https://github.com/vllm-project/vllm>, 2024.

[55] Tensorrt-llm. <https://github.com/NVIDIA/TensorRT-LLM>, 2024.